Title:

Tailoring Phonon Polaritons in hBN with the Plasmonic Phase-Change Material In_3SbTe_2

Author(s) and Corresponding Author(s)*:

Lina Jäckering*,+,1, Aaron Moos+,1, Lukas Conrads[1], Yiheng Li[1], Alexander Rothstein[2,3], Dominique Malik[1], Kenji Watanabe[4], Takashi Taniguchi[5], Matthias Wuttig[1,6,7], Christoph Stampfer[2,3,7], Thomas Taubner*,1

*jaeckering@physik.rwth-aachen.de; taubner@physik.rwth-aachen.de

+both authors contributed equally

Affiliations

[1]1st Institute of Physics (IA), RWTH Aachen University, 52074 Aachen, Germany

[2]2nd Institute of Physics, RWTH Aachen University, 52074 Aachen, Germany

[3]Peter Grünberg Institut (PGI-9), Forschungszentrum Jülich, 52425 Jülich, Germany

[4]Research Center for Electronic and Optical Materials, National Institute for Materials Science, 1-1 Namiki, Tsukuba 305-0044, Japan

[5]International Center for Materials Nanoarchitectonics, National Institute for Materials Science, 1-1 Namiki, Tsukuba 305-0044, Japan

[6] Peter Grünberg Institut (PGI-10), Forschungszentrum Jülich, 52425 Jülich, Germany

[7]Juelich-Aachen Research Alliance (JARA-FIT), 52425 Juelich, Germany

Abstract:

Polaritons in van-der-Waals materials (vdWM) promise high confinement and multiple tailoring options by resonators and launching structures which conventionally require cumbersome lithography techniques. Optical programming of phase-change materials (PCMs) offers fast and reconfigurable fabrication of these structures. As the plasmonic PCM In_3SbTe_2 can be switched between a dielectric and metallic phase, In_3SbTe_2 is promising for optical programming of metallic launching structures to tailor and confine polaritons in vdWM. Here, we combine the vdWM hexagonal boron nitride (hBN) with In_3SbTe_2 and optically program circular resonators for hBN's phonon polaritons into In_3SbTe_2. We investigate the polariton resonators with near-field optical microscopy. Demonstrating the reconfigurability, we decrease the resonator diameter to increase the confinement up to $\lambda/39$ and achieve a quality factor of 72. Finally, we fabricate a focusing structure for hBN's polaritons whose focal point we reconfigure. We promote In_3SbTe_2 as a versatile platform for rapid prototyping of polariton optics in vdWM.

Keywords: hBN, phonon polaritons, resonator, reconfigurable, In_3SbTe_2

Many nanophotonic devices are based on the hybridization of photons with polarization charges in a material, e.g. plasmons in a metal or phonons in a polar crystal. This hybridization results in a confined quasiparticle called polariton.[1] In recent years, interest in nanophotonics has been drawn to van der Waals materials (vdWM) as they host polaritons with high confinement, long propagation length and they can easily be combined to heterostructures.[2,3]

Improving nanophotonic devices requires advanced manipulation of polariton propagation and their enhanced confinements.[3] The polariton propagation can be manipulated by their coupling to optical structures, e.g., resonators[4–6], or by changing the dielectric environment[7–9]. The manipulation of propagation allows for optical waveguiding and lensing whereas a high confinement by resonators is interesting for molecular sensing.[2,3] However, most of the optical structures rely on cumbersome fabrication techniques.

Conventionally, micrometer-sized optical structures for polaritons in vdWM are either fabricated by directly etching the vdWM or by precisely aligning the vdWM flake with a pre-defined structure of, e.g., gold. Both fabrication options require several process steps including flake transfer, careful alignment of the flake, e-beam or focused ion beam, lithography, and etching.[5,6,10–13] Several of those techniques require the access to clean room facilities. Apart from being time-consuming, a further drawback of conventional fabrication techniques is that—once fabricated—the structures cannot be changed or adapted.[5,6,10–13] Relying on conventional fabrication techniques hinders fast prototyping and adaption of optical structures for polaritons.

Tunable polariton optics have been realized relying on phase transitions or tunable conductivities of the substrate of the polariton-hosting material. For example, the volatile phase transition of VO_2 upon heating has been employed to tailor the propagation of hyperbolic phonon polaritons (HPhP) in hexagonal boron nitride (hBN).[14] Conventionally fabricated hBN resonators have been transferred onto graphene whose conductivity is gate-tunable to create a gate-tunable resonator.[13] These choices of substrates, however, do still require either the careful alignment of the hBN flake

to conventionally fabricated nanostructures into the tunable substrate or careful alignment of conventionally nanostructured hBN onto the tunable substrate. Further, hBN has been transferred onto resonator structures of different conductivity locally programmed into the oxide $SmNiO_3$ (SNO) by applying local high electric fields with an conductive atomic force microscope.[15] Although SNO allows for local programming of structures and tailoring of its conductivity, the programming, reconfiguring or tuning of resonators after hBN flake deposition has not been demonstrated. These previous choices of substrates thus do not yet offer fast-prototyping of reconfigurable optical structures.

Fast prototyping of reconfigurable micrometer-sized structures can be realized with phase-change materials (PCMs). PCMs offer non-volatile switching between two (meta-) stable phases, the amorphous and the crystalline phase, which exhibit distinct permittivities.[16,17] The reversible phase change can be induced by local heating of the PCM, e.g., by electrical or optical pulses.[16] A pulsed laser can be used to locally switch the PCM and thereby optically program mircometer-sized structures. In contrast to conventional fabrication techniques, only a fast two-step process is required, i.e. the vdWM flake is exfoliated onto the PCM and the optical structure is programmed, no clean-room techniques are needed, and the structures are reconfigurable.

In the past, most applications of PCMs in the field of nanophotonics relied on a combination of a bulk, surface-polariton-hosting material with the PCM $Ge_3Sb_2Te_6$ (GST). GST has two dielectric phases and therefore allows for a change of the dielectric environment.[16] This change of the dielectric environment has been exploited to investigate switchable and reconfigurable surface phonon polariton (SPhP) resonators.[18,19] The PCM GST has also been introduced to polaritonics with vdWM by exploiting the permittivity change of GST to modulate the propagation of HPhPs in hBN that are launched at a flake edge. For example, planar lenses have been programmed by locally crystallizing GST and thereby providing a permittivity change between amorphous and crystalline GST of about 25 from 12 to 37 for their real parts between 1350 and 1650 cm^{-1}.[7]

In contrast, the plasmonic PCM In_3SbTe_2 (IST) offers a phase change between the dielectric amorphous ($\varepsilon > 0$) and the metallic crystalline phase ($\varepsilon < 0$) making it a promising platform for reconfigurable polariton launching structures.[20–22] IST has been extensively studied for antenna resonance tuning, tailoring thermal emission and even for programming large-area infrared beam-shaping metasurfaces.[23–29] Recently, its capability to confine SPhPs into cavities directly written into IST has been demonstrated for the SPhPs-hosting bulk material SiC.[21] In contrast to the surface-confined SPhPs in SiC, the HPhPs in hBN propagate through the hBN slab forming volume-confined modes. The efficient launching of HPhPs in hBN at a phase boundary of IST has been demonstrated—owing to the huge permittivity change from 14 to -133 of 147 in their real part between 1350 and 1650 cm^{-1} when switching IST from the dielectric amorphous to the metallic crystalline phase.[9] As the crystalline phase of IST is metallic it provides a high field confinement.[9] However, resonators imprinted in PCMs for polaritons in vdWM have not been investigated. Here, we continue exploring the arising platform for the versatile tuning of polaritons in vdWM with IST. We study the confinement of hBN's HPhPs into a circular resonator optically programmed into the IST after exfoliation the hBN flake. Further, we demonstrate the capability of reconfiguring the resonator size which allows, for example, to increase the field confinement. Finally, we show polariton focusing with an optically programmed arc structure. In a subsequent post-processing adaptation of the arc structure, we shift the focus point.

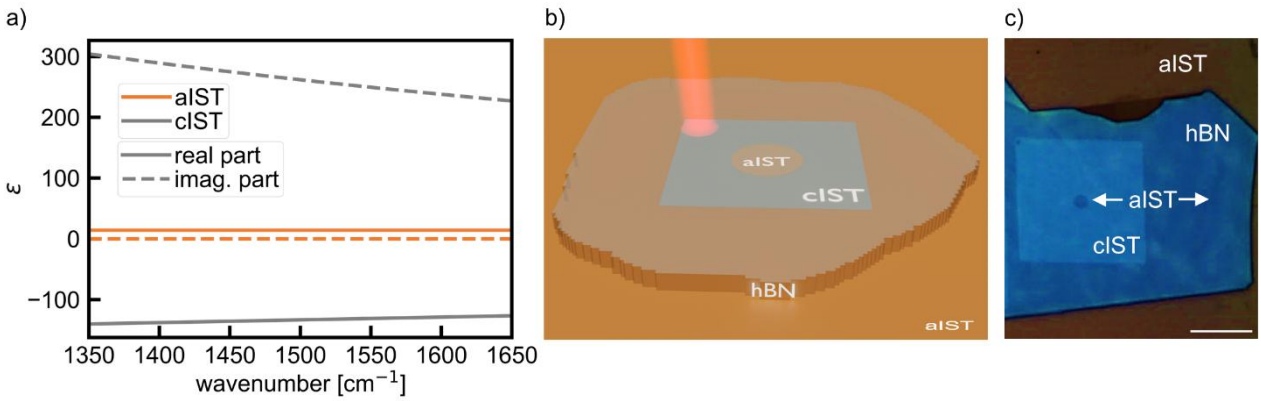


Figure 1: Direct programming of hBN phonon polariton resonators into IST. *a) Real (solid) and imaginary (dashed) part of the permittivity of IST's dielectric amorphous (orange) and metallic crystalline (grey) phase. b) Sketch of the laser crystallization process of the PCM IST for optical programming of an amorphous resonator into the IST below hBN. c) Light microscope image of the rectangular laser-crystallized field in the IST below the 83 nm thick hBN flake (blue) leaving a circular amorphous resonator in the center. The scale bar is 10 µm.*

We design circular resonators by exploiting the two reversibly switchable phases of IST. While the amorphous phase has a slightly positive real part of the permittivity, the crystalline phase has a strongly negative real part following a Drude-like behavior and thereby demonstrating its metallic behavior (c.f. Figure 1a). We crystallize the amorphous IST below the hBN flake (d_{hBN} = 83 nm) with precise laser pulses to create a circular amorphous resonator (c.f. sketch in Figure 1b and light microscope image in Figure 1c). To crystallize the IST, we use a pulsed laser diode with a wavelength of 660 nm. At this wavelength the hBN is highly transparent. This allows us to create laser-crystallized spots through the hBN in the IST below. Due to the elliptical beam profile, we create elliptically crystallized spots that we spatially overlay to program an amorphous resonator. The time to write the field of crystalline laser spots leaving an amorphous resonator (see Figure 1c) takes about 10 minutes. This fast prototyping allows us to study resonators for hBN flakes of various thicknesses. We find that we can optically program resonators into the IST through hBN flakes with thicknesses ranging from 35 to 465 nm (see Supplementary Note 1).

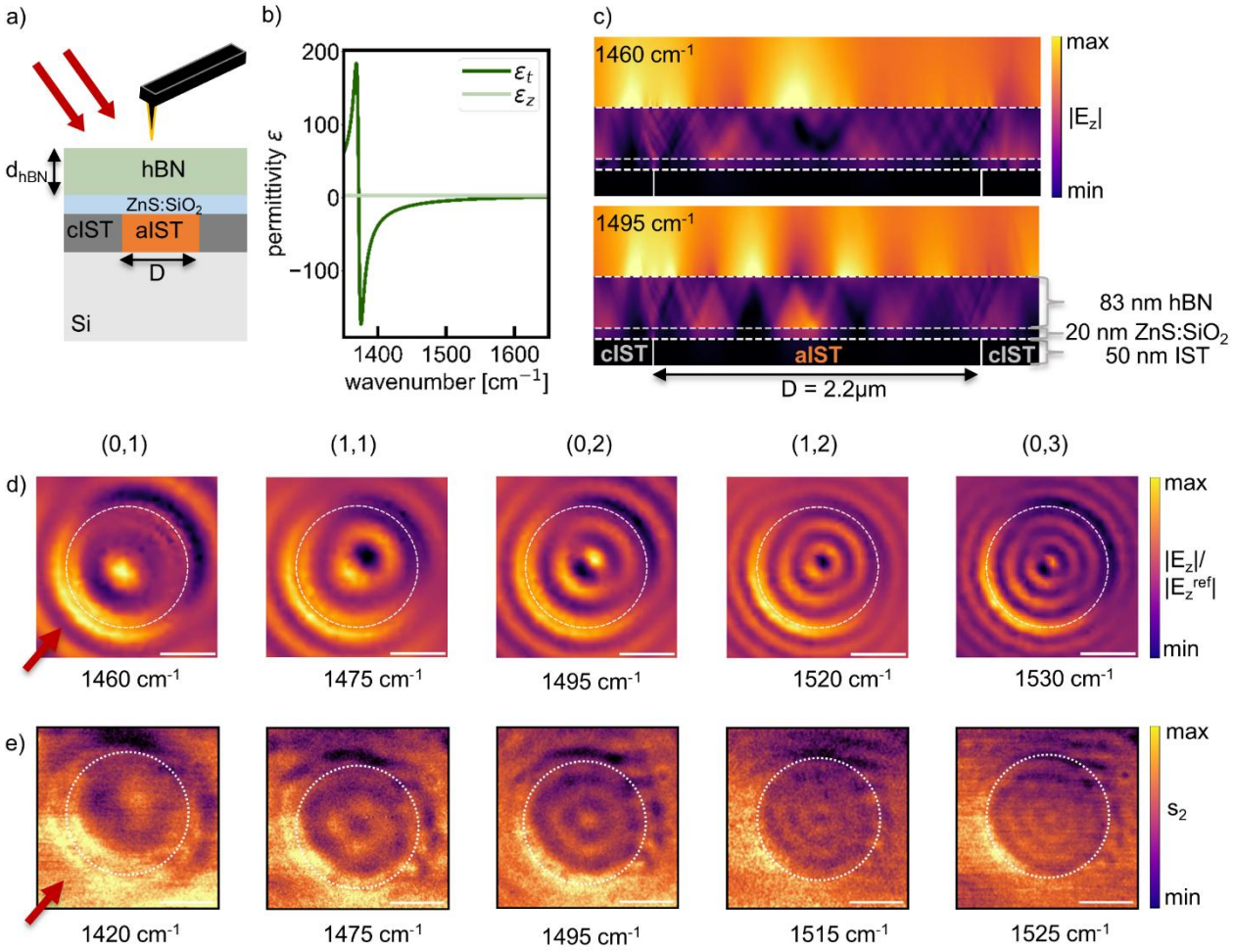


Figure 2: Direct imaging of the resonator modes of hBN phonon polariton resonators programmed into IST. *a) Sketch of the s-SNOM imaging of modes in the amorphous resonator structure for HPhPs in hBN (d_{hBN} = 83 nm) written into IST as a side view. b) In-plane (dark green) and out-of-plane (light green) permittivity of hBN in the investigated upper reststrahlenband (permittivity taken from ref.[30]). c) Cross section of the simulated HPhP mode behavior in the hBN above the amorphous resonator structure (D = 2.2 µm). d) Simulations of the electric field of the resonator modes at five different wavenumbers showing various resonator modes. e) s-SNOM amplitude images of hBN's HPhPs at the same modes as in d). The red arrows in d) and e) indicate the in-plane illumination direction of the incident laser. The scale bars correspond to 1 µm.*

First, we investigate the resonator modes of hBN's HPhPs in the upper reststrahlenband with scattering-type scanning near-field optical microscopy (s-SNOM) which is sensitive to local near-fields, e.g. propagating and localized polaritons, and enables a wavelength-independent resolution down to 10 nm.[31] In s-SNOM, a sharp tip is brought into proximity to the sample surface and illuminated with laser light (c.f. Figure 2a). Acting as an optical antenna, the tip strongly

enhances the electric fields. The scattered field is detected interferometrically to obtain the amplitude s_n and the phase φ_n, here n indicates the demodulation order.

The polaritonic near-fields at the hBN surface that we can image with s-SNOM (see sketch in Figure 2a) originate from hBN's volume-confined phonon polaritons and are tailored by the IST below. hBN has an anisotropic crystal structure as it has polar bonds in-plane but van-der Waals bonds out-of-plane. Therefore, hBN has different permittivities along the in- and out-of-plane axes (shown in Figure 2b), which are not only different but also opposite in sign. This leads to hyperbolic isofrequency curves for hBN's hyperbolic phonon polaritons (see Supplementary Note 2) and defines hBN as a natural hyperbolic material.[11,32–35] The HPhPs show a propagation behavior distinct from polaritons in isotropic materials. While in isotropic materials the photon wavenumber defines the magnitude of the polariton wavevector, in hyperbolic materials the magnitude of the polariton wavevector can be arbitrarily high but the angle of polariton propagation is defined. The HPhPs propagate under a restricted angle through the hBN slab and are reflected at the interfaces of the slab. The HPhPs form volume-confined modes similar to waveguide modes[11,32,34] (see Supplementary Note 2 for a detailed introduction to hBN's HPhPs). Further, the HPhPs in hBN feature the hyperlensing effect allowing for super-resolution and enlarged imaging of structures below the hBN.[11,34,36,37]

As introduced in Figure 1, we now combine hBN with IST that can be switched between two phases with distinct permittivities. By changing the permittivity of the material below hBN, we can modify the propagation behavior of hBN's HPhP (see Supplementary Note 3 for experimental and theoretical dispersions). We optically program local amorphous circular structures into IST which serve as resonators for the HPhPs propagating in the hBN above the IST. In the used layer stack (see Figure 2a) the IST is capped by a layer of $ZnS:SiO_2$ to prevent the IST from oxidation.

The electric fields simulated (see Methods) in a cross section across the hBN IST heterostructure in Figure 2c demonstrate that the HPhPs are confined within the hBN slab and propagate only

under a restricted angle. The simulations show that the polaritons are launched at the boundary between crystalline and amorphous IST and propagate in both directions away from the boundary. For increasing wavenumber (bottom in Figure 2c) the propagation angle of the confined polaritons decreases.[11,34] The confined polariton propagation within the hBN slab transfers into a periodic pattern of high fields above the hBN slab. In a top view, this pattern of high fields corresponds to the appearance of rings of high fields due to the circularly symmetric geometry of the resonator (c.f. simulations in Figure 2d). The field patterns in our simulations are asymmetric due to the considered illumination direction from the left bottom marked by the red arrow that resembles the illumination direction of the s-SNOM measurements shown in Figure 2e. In the simulation at 1460 cm^{-1}, we observe a single spot of high fields in the center of the resonator. With increasing wavenumber at 1475 cm^{-1}, this spot evolves into a ring of high fields with a minimum in its center. For further increasing wavenumbers (1495 -1530 cm^{-1}), we observe alternating maxima and minima in the center of the resonator and an increasing number of rings of high fields. The observation of rings of high fields with alternating minima and maxima in the center is in agreement with results on circular resonators for SPhPs and interpreted as the evolution of modes in this resonator.[18,21,38] Theoretically, the modes of such circular resonators for surface polaritons can be calculated by $k_p D + \phi = 2x_n(J_m)$, where k_p is the polariton wavevector, D the resonator diameter, ϕ the reflection phase at the resonator boundaries and $x_n(J_m)$ the n-th root of the Bessel function of first kind and order m J_m.[39] Consequently, the observed modes are denoted as (n,m). We attribute the observed evolution of modes in the resonator for the HPhPs to the evolution from the (0,1) mode at 1460 cm^{-1} to the (0,3) mode at 1530 cm^{-1}.

Our s-SNOM amplitude images (Figure 2e) validate this confinement of the polaritons experimentally as the s-SNOM amplitude images of the resonator at different wavenumbers between 1420 and 1525 cm^{-1} reveal the evolution of the same resonator modes from (0,1) to (0,3). We find a good agreement with the simulated field patterns. Thereby, we demonstrate direct programming of resonator structures for hBN's HPhPs into IST, extending the recently opened

platform of programming resonators into IST for surface PhPs in bulk materials[21] to volume-confined hyperbolic PhPs in vdWM. Simultaneously, we extend the portfolio of systematically studied reconfigurable polariton optics for hBN to resonators formerly restricted to refractive optics.

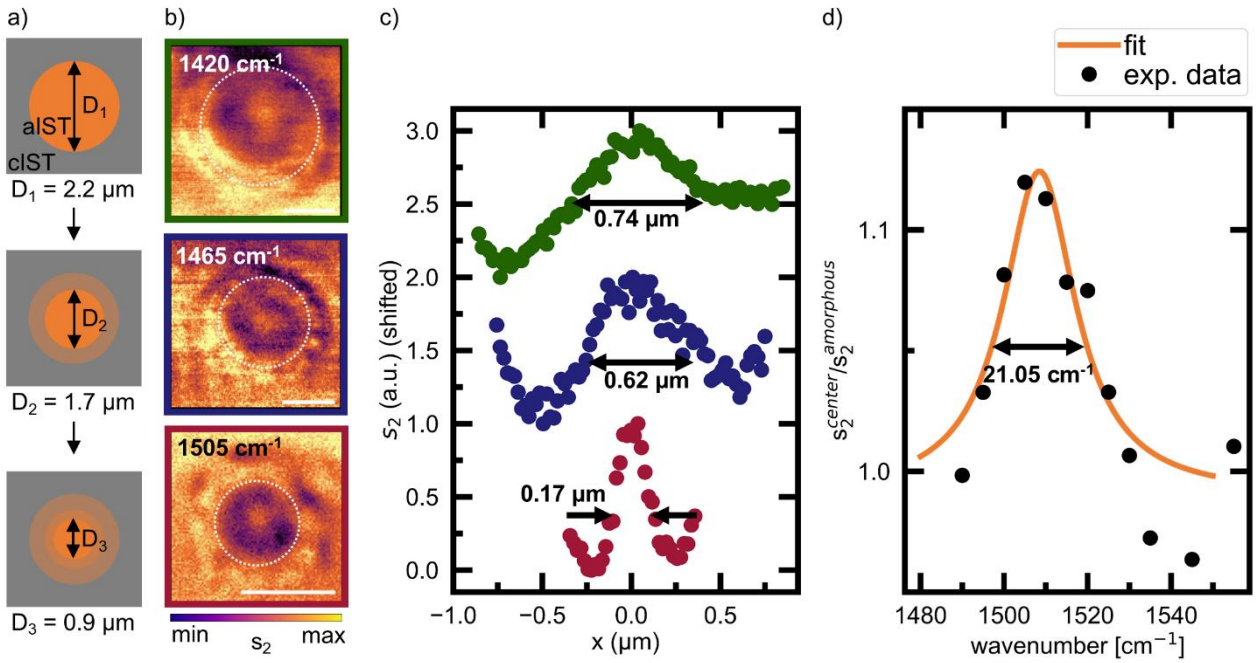


Figure 3: Reconfiguring the resonator diameter allows for tailoring the polariton confinement: *a) By laser crystallization the diameter D_1 of the programmed resonator is sequentially decreased to D_2 and then D_3. b) s-SNOM amplitude images of the (0,1) resonator mode in an amorphous resonator whose diameter is decreased sequentially from D_1 = 2.2 µm (top, green) to D_3 = 0.9 µm (bottom, red). The scale bars correspond to 1 µm. c) Line profiles of the resonator modes in b) reveal the increasing confinement of the mode for a decreasing resonator diameter from λ/10 to λ/39. The line profiles are shifted for better visibility. The arrows and values correspond to the full-width-half-maximum. d) Normalized s-SNOM amplitude in the center of the resonator displaying the spectral evolution of the (0,1) mode of the resonator with diameter D_3 = 0.9 µm (additional s-SNOM images at different wavenumbers shown in Supplementary Note 4). From fitting the experimental data (black dots) with a Lorentzian function (orange solid line) we determined the full-width-half-maximum (indicated by the arrow) to be 21.05 cm^{-1} and the resonant wavenumber to be 1508.48 cm^{-1}, resulting in a quality factor of 72.*

Next, we reconfigure the resonator diameter by additional laser crystallization as sketched in Figure 3a. We sequentially decrease the diameter from D_1 = 2.2 µm to D_2 = 1.7 µm and finally D_3 = 0.9 µm. With s-SNOM we visualize the (0,1) mode where we observe a single maximum in the center of the resonator for each diameter that appears at higher wavenumbers for decreasing diameters (c.f. Figure 3b). By decreasing the diameter, the full-width-half-maximum (FWHM) of

the peak in the center decreases from 0.74 to 0.17 μm (c.f. Figure 3c), demonstrating a strong confinement of the polaritons in the amorphous resonator structure written into IST. We find an enhancement of the confinement $\frac{\lambda_0}{FWHM}$ from 10 for the largest resonator (D_1 = 2.2 μm) to 39 for the smallest resonator (D_3 = 0.9 μm). To further quantify the performance of optically programmed resonators, we determine the quality factor of the (0,1) mode of the smallest resonator (D_3 = 0.9 μm). We perform sequential s-SNOM spectroscopy (c.f. Supplementary Note 4) and from the s-SNOM amplitude images we extract the normalized amplitude in the center of the resonator. The spectral evolution of the s-SNOM amplitude in Figure 3d reveals a maximal amplitude at about 1508 cm^{-1} that corresponds to the resonance wavenumber of the (0,1) mode. We determine the full-width-half-maximum of the (0,1) mode by fitting the experimental data with a Lorentzian function (red solid line) to be 21.05 cm^{-1}. The quality factor is subsequently determined to be $Q = \frac{\nu_{res}}{FWHM}$~72. The performance of resonators for HPhP in hBN optically programmed into the IST is comparable to conventionally fabricated tunable resonators for HPhP in hBN[13] and to reconfigurable resonators for bulk polariton-hosting materials[18,19,21] (c.f. comparative study in Supplementary Note 6).

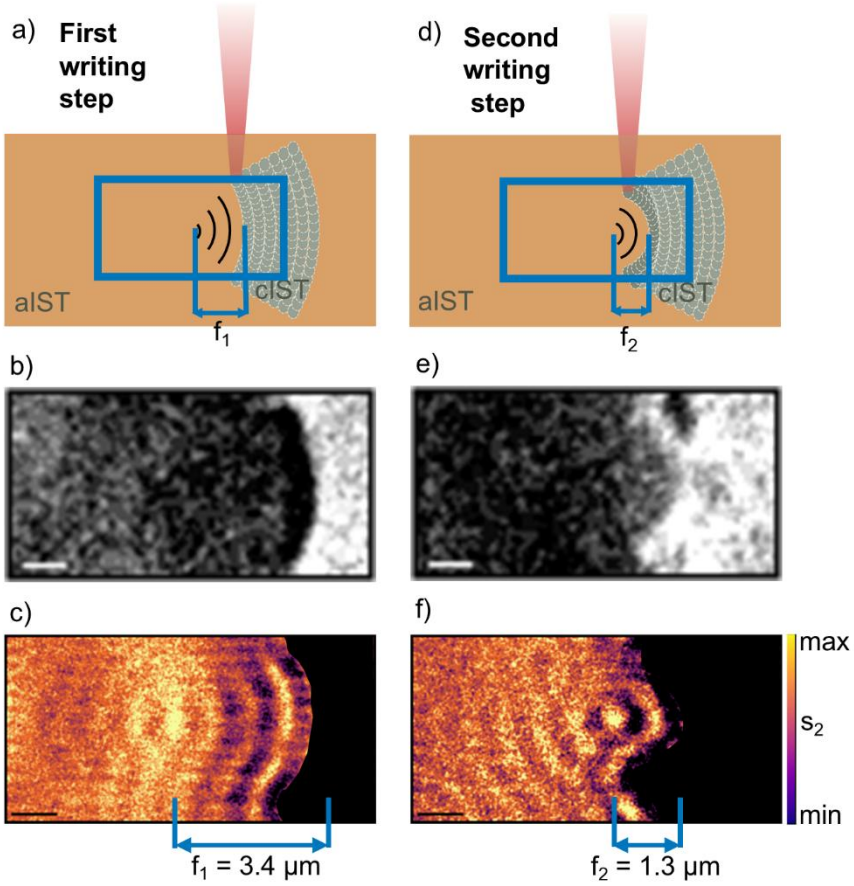


Figure 4: Reconfigurable focusing of phonon polaritons in hBN*. a) Sketch of a launching arc structure directly written into IST by laser crystallization. The black lines indicate the wavefronts of HPhPs launched by the structure. b) Light microscope image of the crystalline launching arc structure below hBN corresponding to the area marked by the blue rectangle in a). c) s-SNOM amplitude image taken at 1480 cm^{-1} of hBN's HPhPs launched and focused to 3.4 µm by the launching arc structure.d) Sketch of reconfiguring the arc structure by additional laser crystallization of the IST. The black lines indicate the wavefronts of HPhPs launched by the structure. e) Light microscope image of the reconfigured arc structure with a decreased curvature radius corresponding to the area marked by the blue rectangle in d). f) s-SNOM amplitude image taken at 1480 cm^{-1} of hBN's HPhPs launched and focused to 1.3 µm by the reconfigured launching arc structure. The scale bars correspond to 1 µm.*

Finally, we program a crystalline arc structure into the IST below a 102 nm thick hBN flake as sketched in Figure 4a. The arc structure is designed to focus hBN's HPhPs as the black sketched wave fronts indicate. Our design was inspired by Huber et al.[40] who fabricated a gold arc structure on SiC by conventional fabrication techniques to focus the SPhPs in SiC. The optical light microscope image (Figure 4b) of the area marked with a blue rectangle in Figure 4a shows a bright arc structure corresponding to the crystallized area. This arc structure is designed with an inner

radius of 3 μm such that it focusses the HPhPs onto a focal point with a focal length of 3 μm. The s-SNOM amplitude image in Figure 4c reveals a fringe pattern that tapers towards the left until a focal point at about 3.4 μm distance from the arc structure is observed. Further to the left the fringe pattern widens and flattens out. The fringe pattern arises from the interference of the incident light and the HPhPs in hBN launched at the boundary of the crystalline IST structure. This interference might explain the deviation from the expected focal length.

Now, we aim for a change of the focal length towards 1 μm. Therefore, we perform a 2nd, post-processing writing process as sketched in Figure 4d. We now change the inner curvature radius of the arc structure to 1 μm such that the HPhPs are focused to a point closer to the launching structure as indicated by the sketched wavefronts. The optical light microscope image in Figure 4e shows the modified crystalline arc structure with a smaller curvature radius. The s-SNOM amplitude image in Figure 4f reveals a bright fringe close to the arc structure and a bright spot at a distance of about 1.3 μm. The reconfigured arc structure now focusses hBN's HPhPs to a focal point of 1.3 μm. The electric field simulations in Supplementary Note 5 support our experimental observations. By reconfiguring the crystalline arc structure, we have adapted the focal length of our focusing structure within a single post-processing step. The easy reconfigurability makes IST a versatile and flexible platform to study polariton modification by optical launching structures.

We demonstrate circular resonator structures directly written into IST below hBN by laser crystallization. The confined resonator modes are visualized with near-field optical microscopy. We decrease the resonator diameter and thereby increase the mode confinement to $\frac{\lambda_0}{39}$ to showcase the reconfigurability of the programmed structures. The direct programming of resonator structures enables fast prototyping that we exploit to program resonators for hBN thicknesses ranging from 35 to 465 nm (see Supplementary Note 1). For all thicknesses the resonator modes can be identified demonstrating the versatility of the hBN IST platform. Finally, we program a crystalline focussing structure with a focal length of 3.4 μm into the IST in order to

focus the HPhPs. By post-processing, meaning a further crystallization process, we adapt the focal length to 1.3 µm.

Our reconfigurable resonators for polaritons in hBN show a confinement $\left(\frac{\lambda_0}{39}\right)$ and quality factor (Q~72) comparable to that of previously investigated tunable but volatile resonators for polaritons in hBN[13] as well as reconfigurable resonators for bulk polariton-hosting materials[18,19,21]. We envision even better performance of our reconfigurable resonators when further shrinking the resonator diameter, using thinner hBN and isotopically enriched hBN[41]. Thereby, we extend the portfolio of reconfigurable structures for polaritons in hBN that was previously restricted to extended phase boundaries[9,14,15], refractive structures[7] and conceptional demonstration of triangular resonators[15] (c.f. Supplementary Note 6).

Optical structures written into IST are not limited to resonators. In principle, much more complex launching structures such as metasurfaces to steer polaritons can be programmed into IST similar to those written into GST[7]. As IST allows for fast prototyping of launching structures through vdWM of various thicknesses, we expect IST to be a versatile substrate where optical structures for polaritons in vdWM can be directly imprinted. With this method we shrink down the time-consuming multi-step fabrication process of optical structures to a fast two-step process, i.e. the exfoliation of the vdWM onto the IST and the subsequent optical programming of the desired structure into the IST. Thereby, IST can facilitate the exploration of polaritons in other exciting in-plane anisotropic vdWM such as α-MoO_3[42,43], β-Ga_2O_3[44], $MoOCl_2$[45] and their heterostructures. Apart from reconfiguring the programmed structures, a second modulation of the polaritons could be added by stacking the phonon-polariton-hosting materials into heterostructures with graphene since the resulting hybrid phonon plasmon polaritons are gate-tunable[46].

Supporting Information

The Supporting Information (PDF) include Methods and Supplementary Notes on fast prototyping of resonators written into IST below hBN flakes of various thicknesses, hyperbolic phonon polaritons, dispersion of hyperbolic phonon polaritons in hBN on amorphous and crystalline IST, analysis of the quality factor of an optically programmed resonator into IST below hBN, simulation of reconfigurable focusing of polaritons in hBN by a launching arc structure, and comparative study of reconfigurable polariton optics and polariton resonators.

Acknowledgements

The authors thank Maike Kreutz for the sputter deposition of the thin film layer stack. L.J. acknowledges the support of RWTH University through the RWTH Graduate Support scholarship. L.J., L.C. and T.T. acknowledge support by the Deutsche Forschungsgemeinschaft (DFG No. 518913417 & SFB 917 “Nanoswitches”). M.W. acknowledges support by the Deutsche Forschungsgemeinschaft (SFB 917 “Nanoswitches”). A.R. and C.S. acknowledge support from the European Union’s Horizon 2020 research and innovation programme under grant agreement no. 881603 (Graphene Flagship), the Deutsche Forschungsgemeinschaft (DFG, German Research Foundation) under Germany’s Excellence Strategy - Cluster of Excellence Matter and Light for Quantum Computing (ML4Q) EXC 2004/1-390534769, the FLAG-ERA grant PhotoTBG, by the Deutsche Forschungsgemeinschaft (DFG, German Research Foundation) - 471733165. K.W. and Ta.Ta. acknowledge support from the JSPS KAKENHI (Grant Numbers 20H00354 and 23H02052) and World Premier International Research Center Initiative (WPI), MEXT, Japan.

References

1. Solymar, L. & Shamonina, E. *Waves in metamaterials* (Oxford University Press, Oxford, New York, 2009. ISBN: 9780199215331).

2. Zhang, Q. *et al.* Interface nano-optics with van der Waals polaritons. *Nature* **597,** 187–195; 10.1038/s41586-021-03581-5 (2021).

3. Guo, X. *et al.* Polaritons in Van der Waals Heterostructures. *Advanced Materials* **35,** e2201856; 10.1002/adma.202201856 (2023).

4. Tamagnone, M. *et al.* High quality factor polariton resonators using van der Waals materials. *arXiv*. October 1, 2020; 10.48550/arXiv.1905.02177v2 (accessed 2025-03-04).

5. Tamagnone, M. *et al.* Ultra-confined mid-infrared resonant phonon polaritons in van der Waals nanostructures. *Science advances* **4,** eaat7189; 10.1126/sciadv.aat7189 (2018).

6. Herzig Sheinfux, H. *et al.* High-quality nanocavities through multimodal confinement of hyperbolic polaritons in hexagonal boron nitride. *Nature materials* **23,** 499–505; 10.1038/s41563-023-01785-w (2024).

7. Chaudhary, K. *et al.* Polariton nanophotonics using phase-change materials. *Nature communications* **10,** 4487; 10.1038/s41467-019-12439-4 (2019).

8. Menabde, S. G. *et al.* Near-field probing of image phonon-polaritons in hexagonal boron nitride on gold crystals. *Science advances* **8,** eabn0627; 10.1126/sciadv.abn0627 (2022).

9. Lu, D. *et al.* Tunable hyperbolic polaritons with plasmonic phase-change material In 3 SbTe 2. *Nanophotonics* **13,** 937–944; 10.1515/nanoph-2023-0911 (2024).

10. Dai, S. *et al.* Manipulation and Steering of Hyperbolic Surface Polaritons in Hexagonal Boron Nitride. *Advanced Materials* **30,** e1706358; 10.1002/adma.201706358 (2018).

11. Dai, S. *et al.* Subdiffractional focusing and guiding of polaritonic rays in a natural hyperbolic material. *Nature communications* **6,** 6963; 10.1038/ncomms7963 (2015).

12. Duan, J. *et al.* Launching Phonon Polaritons by Natural Boron Nitride Wrinkles with Modifiable Dispersion by Dielectric Environments. *Advanced Materials* **29,** 1702494; 10.1002/adma.201702494 (2017).

13. Duan, J. *et al.* Active and Passive Tuning of Ultranarrow Resonances in Polaritonic Nanoantennas. *Advanced Materials* **34,** e2104954; 10.1002/adma.202104954 (2022).

14. Folland, T. G. *et al.* Reconfigurable infrared hyperbolic metasurfaces using phase change materials. *Nature communications* **9,** 4371; 10.1038/s41467-018-06858-y (2018).

15. Aghamiri, N. A. *et al.* Reconfigurable hyperbolic polaritonics with correlated oxide metasurfaces. *Nature communications* **13,** 4511; 10.1038/s41467-022-32287-z (2022).

16. Wuttig, M., Bhaskaran, H. & Taubner, T. Phase-change materials for non-volatile photonic applications. *Nature Photon* **11,** 465–476; 10.1038/nphoton.2017.126 (2017).

17. Wuttig, M. *et al.* Revisiting the Nature of Chemical Bonding in Chalcogenides to Explain and Design their Properties. *Advanced Materials* **35,** e2208485; 10.1002/adma.202208485 (2023).

18. Sumikura, H. *et al.* Highly Confined and Switchable Mid-Infrared Surface Phonon Polariton Resonances of Planar Circular Cavities with a Phase Change Material. *Nano letters* **19,** 2549–2554; 10.1021/acs.nanolett.9b00304 (2019).

19. Li, P. *et al.* Reversible optical switching of highly confined phonon-polaritons with an ultrathin phase-change material. *Nature materials* **15,** 870–875; 10.1038/nmat4649 (2016).

20. Heßler, A. *et al.* In3SbTe2 as a programmable nanophotonics material platform for the infrared. *Nature communications* **12,** 924; 10.1038/s41467-021-21175-7 (2021).

21. Conrads, L., Schüler, L., Wirth, K. G., Wuttig, M. & Taubner, T. Direct programming of confined surface phonon polariton resonators with the plasmonic phase-change material In3SbTe2. *Nat Commun* **15,** 3472; 10.1038/s41467-024-47841-0 (2024).

22. Conrads, L. *et al.* Real-space imaging of confined infrared surface plasmon polaritons on doped semiconductors covered with phase-change materials. *Science advances* **11,** eadr6844; 10.1126/sciadv.adr6844 (2025).

23. Heßler, A. *et al.* Nanostructured In3SbTe2 antennas enable switching from sharp dielectric to broad plasmonic resonances. *Nanophotonics* **11,** 3871–3882; 10.1515/nanoph-2022-0041 (2022).

24. Heßler, A., Conrads, L., Wirth, K. G., Wuttig, M. & Taubner, T. Reconfiguring Magnetic Infrared Resonances with the Plasmonic Phase-Change Material In 3 SbTe 2. *ACS photonics* **9,** 1821–1828; 10.1021/acsphotonics.2c00432 (2022).

25. Conrads, L. *et al.* Reconfigurable and Polarization-Dependent Grating Absorber for Large-Area Emissivity Control Based on the Plasmonic Phase-Change Material In 3 SbTe 2. *Advanced Optical Materials* **11,** 2202696; 10.1002/adom.202202696 (2023).

26. Meng, C. *et al.* Broadband hyperbolic thermal metasurfaces based on the plasmonic phase-change material In3SbTe2. *Nanoscale* **15,** 6306–6312; 10.1039/d2nr07133a (2023).

27. Zha, W. *et al.* Nonvolatile High-Contrast Whole Long-Wave Infrared Emissivity Switching Based on In 3 SbTe 2. *ACS photonics* **10,** 2165–2172; 10.1021/acsphotonics.2c00714 (2023).

28. Conrads, L. *et al.* Infrared Resonance Tuning of Nanoslit Antennas with Phase-Change Materials. *ACS nano* **17,** 25721–25730; 10.1021/acsnano.3c11121 (2023).

29. Conrads, L. *et al.* Infrared beam-shaping on demand via tailored geometric phase metasurfaces employing the plasmonic phase-change material In3SbTe2. *Nat Commun* **16,** 3698; 10.1038/s41467-025-59122-5 (2025).

30. Woessner, A. *et al.* Highly confined low-loss plasmons in graphene-boron nitride heterostructures. *Nature materials* **14,** 421–425; 10.1038/nmat4169 (2015).

31. Ocelic, N., Huber, A. & Hillenbrand, R. Pseudoheterodyne detection for background-free near-field spectroscopy. *Appl. Phys. Lett.* **89,** 5064–5066; 10.1063/1.2348781 (2006).

32. Caldwell, J. D. *et al.* Sub-diffractional volume-confined polaritons in the natural hyperbolic material hexagonal boron nitride. *Nature communications* **5,** 5221; 10.1038/ncomms6221 (2014).

33. Caldwell, J. D. *et al.* Photonics with hexagonal boron nitride. *Nat Rev Mater* **4,** 552–567; 10.1038/s41578-019-0124-1 (2019).

34. Li, P. *et al.* Hyperbolic phonon-polaritons in boron nitride for near-field optical imaging and focusing. *Nature communications* **6,** 7507; 10.1038/ncomms8507 (2015).

35. Dai, S. *et al.* Tunable Phonon Polaritons in Atomically Thin van der Waals Crystals of Boron Nitride. *Science* **343,** 1125–1129; 10.1126/science.1247212 (2014).

36. Jäckering, L. *et al.* Super-Resolution Imaging of Nanoscale Inhomogeneities in hBN-Covered and Encapsulated Few-Layer Graphene. *Advanced Science* **12,** e2409039; 10.1002/advs.202409039 (2025).

37. He, M. *et al.* Ultrahigh-Resolution, Label-Free Hyperlens Imaging in the Mid-IR. *Nano letters* **21,** 7921–7928; 10.1021/acs.nanolett.1c01808 (2021).

38. Wang, T., Li, P., Hauer, B., Chigrin, D. N. & Taubner, T. Optical properties of single infrared resonant circular microcavities for surface phonon polaritons. *Nano letters* **13,** 5051–5055; 10.1021/nl4020342 (2013).

39. Filter, R., Qi, J., Rockstuhl, C. & Lederer, F. Circular optical nanoantennas: an analytical theory. *Phys. Rev. B* **85,** 125429; 10.1103/PhysRevB.85.125429 (2012).

40. Huber, A. J., Deutsch, B., Novotny, L. & Hillenbrand, R. Focusing of surface phonon polaritons. *Applied Physics Letters* **92,** 203104; 10.1063/1.2930681 (2008).

41. Giles, A. J. *et al.* Ultralow-loss polaritons in isotopically pure boron nitride. *Nature materials* **17,** 134–139; 10.1038/nmat5047 (2018).

42. Ma, W. *et al.* In-plane anisotropic and ultra-low-loss polaritons in a natural van der Waals crystal. *Nature* **562,** 557–562; 10.1038/s41586-018-0618-9 (2018).

43. Zheng, Z. *et al.* A mid-infrared biaxial hyperbolic van der Waals crystal. *Science advances* **5,** eaav8690; 10.1126/sciadv.aav8690 (2019).

44. Passler, N. C. *et al.* Hyperbolic shear polaritons in low-symmetry crystals. *Nature* **602,** 595–600; 10.1038/s41586-021-04328-y (2022).

45. Venturi, G., Mancini, A., Melchioni, N., Chiodini, S. & Ambrosio, A. Visible-frequency hyperbolic plasmon polaritons in a natural van der Waals crystal. *Nature communications* **15,** 9727; 10.1038/s41467-024-53988-7 (2024).

46. Dai, S. *et al.* Graphene on hexagonal boron nitride as a tunable hyperbolic metamaterial. *Nature nanotechnology* **10,** 682–686; 10.1038/nnano.2015.131 (2015).

Author Contributions Statement

L.J., L.C. and T.T. conceived the project. A.R. and D.M. fabricated parts of the samples. A.M. performed the s-SNOM measurement. L.J. and Y.L. produced preliminary data performing s-SNOM measurements. L.J. supervised the s-SNOM measurements. A.M. performed the numerical field simulations under supervision of L.C. L.J., A.M. and L.C. analyzed the data. M.W. provided the sputtering equipment and phase-change material expertise. C.S. supervised A.R. on selected aspects of the sample fabrication, based on expertise in 2D material exfoliation and stacking. K.W. and Ta.Ta. provided high-quality hBN crystals. All authors contributed to writing the manuscript.

Competing Interests Statement

The authors declare no competing financial interest.